Haemophilia
The Official Journal of the World Federation of Hemophilia,
European Association for Haemophilia and Allied Disorders and
the Hemostasis & Thrombosis Research Society

Haemophilia (2014), **20**, 723–731 DOI: 10.1111/hae.12421

ORIGINAL ARTICLE *Laboratory science*

Lack of recombinant factor VIII B-domain induces phospholipid vesicle aggregation: implications for the immunogenicity of factor VIII

K. GRUSHIN,* J. MILLER,* D. DALM,* E. T. PARKER,† J. F. HEALEY,† P. LOLLAR† and S. STOILOVA-MCPHIE*‡

**Department of Neuroscience and Cell Biology University of Texas Medical Branch, Galveston, TX; †Aflac Cancer and Blood Disorders Center, Children's Healthcare of Atlanta, The Department of Pediatrics Emory University, Atlanta, GA; and ‡Sealy Center for Structural Biology and Molecular Biophysics, University of Texas Medical Branch, Galveston, TX, USA*

Summary. Factor VIII (FVIII) is a multidomain blood plasma glycoprotein. Activated FVIII acts as a cofactor to the serine protease factor IXa within the membrane-bound tenase complex assembled on the activated platelet surface. Defect or deficiency in FVIII causes haemophilia A, a severe hereditary bleeding disorder. Intravenous administration of plasma-derived FVIII or recombinant FVIII concentrates restores normal coagulation in haemophilia A patients and is used as an effective therapy. In this work, we studied the biophysical properties of clinically potent recombinant FVIII forms: human FVIII full-length (FVIII-FL), human FVIII B-domain deleted (FVIII-BDD) and porcine FVIII-BDD bound to negatively charged phospholipid vesicles at near-physiological conditions. We used cryo-electron microscopy (Cryo-EM) as a direct method to evaluate the homogeneity and micro-organization of the protein-vesicle suspensions, which are important for FVIII therapeutic properties. Applying concurrent Cryo-EM, circular dichroism and dynamic light scattering studies to the three recombinant FVIII forms when bound to phospholipid vesicles revealed novel properties for their functional, membrane-bound state. The three FVIII constructs have similar activity, secondary structure distribution and bind specifically to negatively charged phospholipid membranes. Human and porcine FVIII-BDD induce strong aggregation of the vesicles, but the human FVIII-FL form does not. The proposed methodology is effective in characterizing and identifying differences in therapeutic recombinant FVIII membrane-bound forms near physiological conditions, because protein-containing aggregates are considered to be a factor in increasing the immunogenicity of protein therapeutics. This will provide better characterization and development of safer and more effective FVIII products with implications for haemophilia A treatment.

Keywords: coagulation factor VIII, cryo-electron microscopy, haemophilia A, immunogenicity, protein-induced vesicle aggregation

Introduction

Haemophilia A is a hereditary X-chromosome linked bleeding disorder due to defective or deficient factor VIII (FVIII), affecting 1 in 5000 males [1]. Human FVIII is expressed as a 2332 amino acid residues single-chain glycoprotein of ~280 kDa, comprising three A, two C and one B-domain, aligned from the N terminus as: A1-A2-B-A3-C1-C2 (Fig. 1a) [2,3]. The A domains are homologous to each other, to the A domains of factor V (FV) (~40% sequence identity) and the copper-binding plasma protein ceruloplasmin (~30% sequence identity) [4,5]. The C domains are part of the lipid-binding discoidin family and share ~35% sequence identity with the C domains of FV. The B-domain is heavily glycosylated and has no known homologues [5]. In solution, plasma-derived FVIII exists as a mixture of heterodimers of a variable-length heavy chain (HC: A1-A2-B) of 90–200 kDa due to fully or partially removed B-domain by limited proteolysis and a constant length light chain (LC: A3-C1-C2) of 80 kDa. The LC and HC are non-covalently bound via metal ions (Fig. 1) [6].

Correspondence: Stoilova-McPhie Svetla, PhD, Department of Neuroscience and Cell Biology; Scientist, Sealy Center for Structural Biology and Molecular Biophysics, University of Texas Medical Branch at Galveston, 301 University Boulevard, Galveston, TX 77555-0620, USA.
Tel.: 409 747 2159; fax: 409 747 2200;
e-mail: svmcphie@utmb.edu

Accepted after revision 26 February 2014

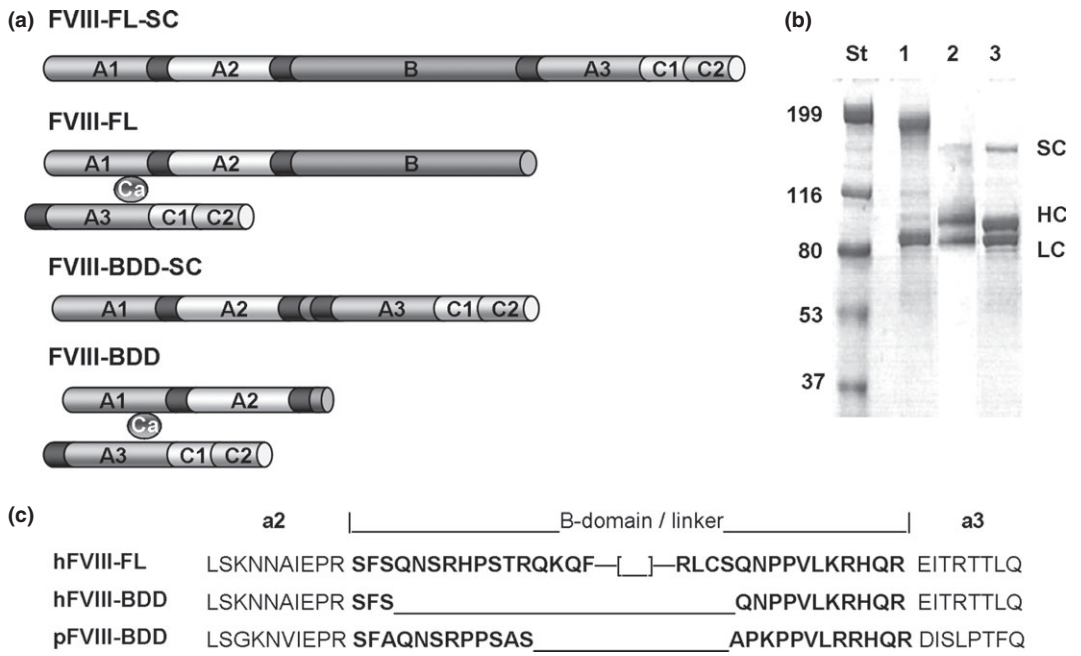

Fig. 1. Primary structure of factor VIII. (a) FVIII-FL-single chain [35] domain organization. The three acidic domains: a1, a2 and a3, important for FVIII proteolytic activation by Thrombin, are indicated with dark grey boxes. FVIII-FL is a mixture of heterodimers of non-covalently linked heavy chain (HC) of the A1-A2-B-domains and a light chain (LC) of the A3-C1-C2. FVIII-BDD-SC and FVIII-BDD heterodimer lacking the B-domain. (b) PAA-SDS gel of FVIII. St indicates the Molecular weight of the standards in kDa. '1' is hFVIII-FL, '2' is hFVIII-BDD and '3' is pFVIII-BDD. The bands corresponding to the FVIII-BDD-SC, the HC and LC are indicated. (c) Amino acid sequence alignment between hFVIII-FL, hFVIII-BDD and pFVIII-BDD at the A2a2___a3A3 level showing the 14 and 24 amino acid linkers introduced for human and porcine FVIII-BDD forms, respectively.

Activated FVIII (FVIIIa) is a cofactor to the serine protease FIXa. Binding of FVIIIa to FIXa onto the activated platelet surface rich in phosphatidylserine (PS) amplifies FIXa proteolytic activity more than 100 000 times, which is necessary for efficient thrombin generation and blood clot formation [7,8]. Both FVIII and FVIIIa bind to PS-rich phospholipid membranes *in vitro*. This property of FVIII is fundamental to its function and to its use as an intravenous drug for haemophilia A [8]. The presence of phospholipids also stabilizes FVIII in solution by increasing its half-life time [9,10]. One of the most effective therapies for haemophilia A is lifelong administration of recombinant human FVIII expressed in mammalian cells without or with parts of the B-domain [11]. The B-domain is dispensable for FVIII procoagulant activity and FVIII-BDD expresses at a higher yield (20-fold) [12,13]. A significant complication of this therapy is the development of inhibitory antibodies to FVIII affecting approximately 30% of haemophilia A patients [14]. Porcine FVIII (pFVIII) concentrate has been used in FVIII inhibitor patients, as pFVIII displays low cross-reactivity with inhibitory antibodies against hFVIII and forms functional complexes with human FIXa [15,16]. Recombinant porcine FVIII-BDD currently is undergoing clinical trials in FVIII inhibitor patients [17]. In addition to antigenic differences, pFVIII has important functional differences from hFVIII. It is more stable in activated form and is expressed at significantly higher levels than hFVIII-BDD [18–20]. Although a 4 Å, low-resolution X-ray crystal structure of hFVIII-BDD has been published [21,22]; no structural information is available for pFVIII.

In this study, we have used cryo-electron microscopy (Cryo-EM), circular dichroism (CD) and dynamic light scattering (DLS) to compare hFVIII-FL, hFVIII-BDD and pFVIII-BDD when free in solution and when bound to phospholipid membranes. We found that, in contrast to hFVIII-FL, hFVIII-BDD and pFVIII form large protein–phospholipid vesicle aggregates, which may contribute to the immunogenicity of FVIII.

Material and methods

FVIII sample preparation

Recombinant hFVIII-FL (Kogenate FS; gift from Bayer Corporation, Berkeley, CA, USA). B-domain deleted human FVIII [23] and porcine FVIII (OL) were expressed in BHK-derived cells and purified as previously described [19]. All proteins were buffer exchanged and concentrated against 20 mM HEPES buffer at pH 7.4 containing 150 mM NaCl and 5 mM $CaCl_2$ through 0.22 μm Millex® GP filter (Millipore, Carrigtwohill, Co. Cork, Ireland) to 2.7 mg mL^{-1} for the hFVIII-FL

and pFVIII-BDD and to 0.7 mg mL^{-1} for the hFVIII-BDD. The protein concentration was monitored with Nanodrop Spectrophotometer ND-1000 (Thermo Fisher Sci Inc, Waltham, MA, USA) and calculated based on the molar absorption coefficient at 280 and 320 nm [24]. Samples were prepared in identical solution conditions and protein to lipid ratios for each of the Cryo-EM, CD, DLS and thrombin generation experiments.

SDS-polyacrylamide gel electrophoresis [25]

Ready Gel® Tris-HCl Gels (4–15%) (Bio-Rad, Hercules, CA, USA) were run according to standard protocols [26]. The gels were stained with GelCode® Blue Stain Reagent (Thermo Scientific, Waltham, MA, USA) and destained with water.

Phospholipid vesicle preparation

PS-containing phosphatidylcholine (PC) vesicles were obtained by mixing PC and PS at a 3:1 (w/w) ratio in $CHCl_3$ (Fisher Scientific, Fair Lawn, NJ, USA). The solvent was evaporated under argon and the lipids solubilized to final concentrations of 1 and 2 mg mL^{-1} in 20 mM HEPES, pH 7.4 containing 150 mM NaCl. The lipid emulsion was extruded several times through a 50-nm polycarbonate membrane filter with LIPOSOFAST-Basic extruder (Glen Creston Ltd, London, UK). The vesicles were stored at 4°C. The 1 mg mL^{-1} solution was used for control and the 2 mg mL^{-1} solution for the protein with vesicle experiments, where the protein and vesicles are mixed at a 1:1 (w/w) ratio.

Thrombin generation assay

Thrombin generation was measured with the Calibrated Automated Thrombogram® System (Diagnostica Stago Inc, Parsippany, NJ, USA) based on Fluoroskan Ascent Analyzer (390 nm excitation, 460 nm emission wavelengths; Thermolabsystems Oy, Helsinki, Finland) [27]. FVIII-deficient plasma (George King Bio-Medical Inc, Overland Park, KS, USA) and normal plasma (Diagnostica Stago Inc) were used as negative and positive controls, respectively. All reagents – PPP Reagent Low, Thrombin Calibrator and FluCa (Fluo-substrate + Fluo-buffer containing Ca^{2+}) – were from CAT assay kits (Thrombinoscope BV, Maastricht, the Netherlands) supplied with a Calibrated Automated Thrombogram® System. The thrombin generation reaction was started by FluCa reagent; in the presence of PPP Reagent Low (1 pM tissue factor and 4 μM phospholipids final plasma concentration), designed to increase sensitivity to factors VIII, IX and XI. Collection and calculation of thrombin activity data were carried out with the Thrombinoscope® software [27].

Circular dichroism

The concentration of hFVIII-FL and pFVIII-BDD proteins in HBS-Ca^{2+} buffer was 1.2 mg mL^{-1} and for hFVIII-BDD was 0.3 mg mL^{-1}. The protein and vesicle samples were mixed at 1:1 (w/w) ratio. CD spectra were acquired with a JASCO-815 CD spectrometer (Easton, MD, USA) in the 180–260 nm range calibrated with d-10 camphor sulphonic acid over the 260–180 nm range. Measurements were carried out in a 0.1 mm path length quartz cuvette under constant nitrogen stream and at room temperature (21°C). Data were collected in continuous scan mode with pitch of 0.1 nm, speed of 50 nm min^{-1} and response time of 2 s. Each spectrum is the average of three accumulations and a bandwidth of 2 nm. Control spectra were recorded for the buffer and the PS-vesicles at the same conditions as for the samples. CD spectra of the protein in the presence and absence of PS-vesicles were calculated with the Jasco-815 software by subtracting the spectra of buffer and protein-free vesicles from the protein and protein + vesicle samples respectively.

Dynamic light scattering

All DLS measurements were carried out with a Zetasizer μV particle analyzer (Malvern Instruments Ltd, Worcester, UK) in a 2-μL volume quartz cuvette, at a light-scattering detection angle of 90° and room temperature (21°C). Each recorded measurement was obtained from 10 consecutive measurements averaged by the Zetasizer Software v6.30. The final particle size and mass distribution were compiled by averaging the data from three independent measurements for the free proteins and vesicles in solution and two independent measurements for the protein bound to vesicle samples.

Cryo-electron microscopy

Cryo-EM samples were prepared by applying 2 μL vesicles and FVIII + vesicle samples onto carbon-coated hydrophilic electron microscopy lacey grids (300 meshes; Ted Pella, Inc., Redding, CA, USA). The excess liquid was blotted and the grids quickly plunged (~2000°C/s) into liquid ethane cooled down by liquid nitrogen to obtain amorphous ice in a Vitrobot Mark IV (FEI, Millsboro, OR, USA). The grids were transferred and observed at liquid nitrogen temperature (−184°C) in a 200 kV JEM2100-LaB6 transmission electron microscope (JEOL Ltd., Tokyo, Japan). Digital micrographs were recorded on a 4096 × 4096 pixel CCD camera (US4000, 15 microns/pixel resolution, Gatan, Inc., Pleasanton, CA, USA) at low electron dose conditions (~16 electrons/$Å^2$), at liquid nitrogen temperature and a final magnification of 52 000×.

Results

FVIII purification and characterization

Human FVIII-FL showed multiple bands on the SDS gels for the HC corresponding to different length of the B-domain with a predominant band of ~200 kDa, including a full size B-domain. Both FVIII-BDD forms consist of a LC of ~80 kDa and a HC of ~90 kDa (Fig. 1b). A single band, more pronounced for the pFVIII-BDD and corresponding to the FVIII-BDD-SC of ~170 kDa, was also resolved [19] (Fig. 1b).

The FVIII activity was estimated with the CAT test [27] (Fig. 2, Table 1). The maximum level of active thrombin generated is the same for the three FVIII forms (Fig. 2). The total amount of thrombin generated during the test (clustered in the 920–1060 nM × min) is reflected by the endogenous thrombin potential (ETP). These results indicate that the efficiency of clot formation for all FVIII forms is similar to that for normal plasma and all proteins characterized in this work are fully functional and intact (Table 1).

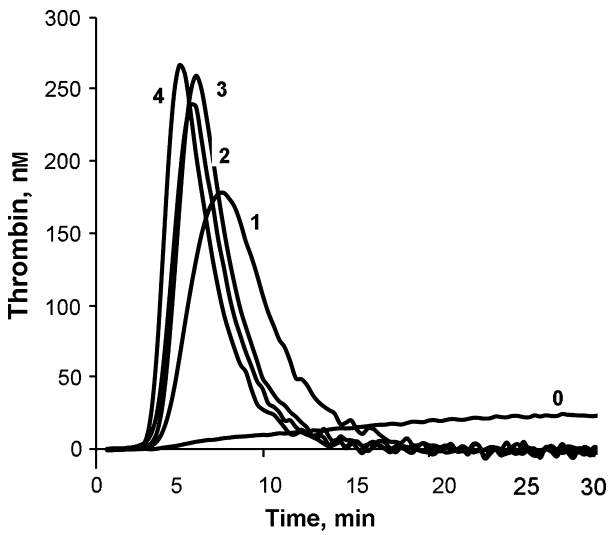

Fig. 2. Activity of FVIII measured as Thrombin generation upon activation of coagulation. Typical FVIII thrombograms for FVIII deficient plasma (0), control blood plasma (1), hFVIII-FL (2), hFVIII-BDD (3) and pFVIII-BDD (4). Each curve is calculated from three independent experiments. The concentration of the recombinant FVIII proteins is two times higher than the FVIII in the normal blood plasma (1 mg mL^{-1}, ~150 μg mL^{-1}).

Table 1. Quantitative parameters for the thrombograms in Fig. 2.

Sample	Lt	ETP (nM × min)	Peak (nM)	TP
pFVIII-BDD	3.2 ± 0.2	955 ± 8	264 ± 6	5.1 ± 0.2
hFVIII-FL	3.7 ± 0	921 ± 8	234 ± 4	6 ± 0
hFVIII-BDD	4.1 ± 0.2	1017 ± 16	258 ± 6	6.22 ± 0.2
Normal plasma	4.3 ± 0	1059 ± 10	177 ± 1	7.67 ± 0
FVIII-deficient plasma	5.1 ± 0.2	0	24 ± 0.3	34 ± 2.4

Data are represented as mean ± SD of three independent experiments. Lt, lag time; ETP, endogenous thrombin potential; Peak, peak height; TP, time to peak.

Circular dichroism

Far UV-CD spectra were measured at closest to physiological conditions: 10 mM HEPES, 150 mM NaCl, 2.5 mM $CaCl_2$, pH 7.4 and room temperature (21°C). The spectra for the hFVIII-FL and pFVIII-BDD are almost identical in the 220–260 range and similar in the 180–220 nm range (Fig. 3a). The broader minimum for the hFVIII-FL form is due to the presence of partial or full B-domain in the HC leading to a population of variable mass FVIII-FL heterodimers, whereas the FVIII-BDD heterodimers are of constant mass and composition (Fig. 1b). This difference was not observed for the FVIII-BDD forms. The similarities in the far UV-CD spectra and secondary structure distribution between the hFVIII-FL and hFVIII-BDD show that the human B-domain is highly disordered and has little to no effect on the overall FVIII secondary structure in solution (Table 2). There are no consistent changes in the CD spectra for the proteins in solution and when bound to PS-vesicles, showing that there are no detectable secondary structure changes upon membrane binding (Fig. 3a). The calculated secondary structure distribution showed a predominant β-strand content of ~36–39% and a low α-helical content of ~4–6%. The distribution was not altered for the protein + vesicle samples and corresponds to the one calculated from the X-ray structure [21] (Table 2).

A homology model for the pFVIII-BDD was built as a template with the hFVIII-BDD crystal structure containing 1261 resolved atoms (3CDZ at 3.98 Å), (Fig. 3b). Because of the high-sequence homology between the two proteins (86%), each amino acid residue in the hFVIII-BDD sequence was mutated to the corresponding amino acid residue in the pFVIII-BDD sequence with the COOT software [28], using the electron density map calculated for the hFVIII-BDD structure (3CDZ) as a restraint [21]. For this purpose, the hFVIII-BDD (FL, uniprot: P00451) and pFVIII-BDD (FL, uniprot: P12263) amino acid sequences were first aligned (Fig. 1c). The C2 domain electron density map from the higher resolution C2 crystal structure (3HNB [29] at 1.7 Å) was used instead of the C2 density map from the 3CDZ crystal structure. Each mutated amino acid side chain was fit according to the highest probability geometry and least clashes with surrounding amino-acid side chains and backbone atoms (Fig. 4b). The pFVIII-BDD homology structure was validated in MolProbity [30].

Dynamic light scattering

Dynamic light scattering studies were carried out for all three FVIII forms in solution and were attached to

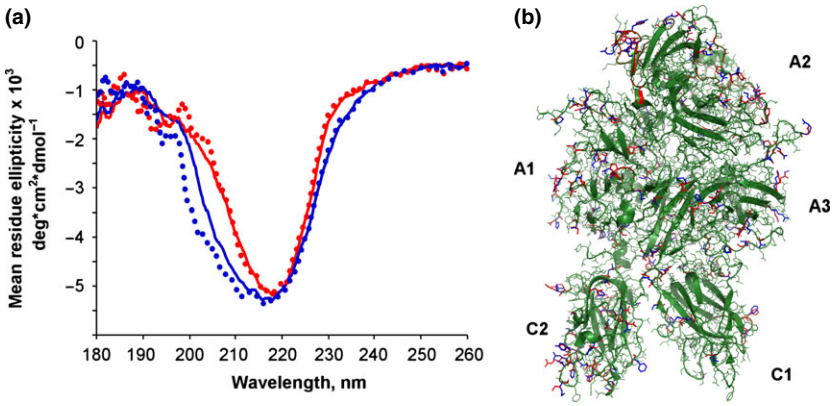

Fig. 3. Secondary and tertiary structure of FVIII. (a) Far UV-CD of hFVIII-FL (blue) and pFVIII-BDD (red). The CD spectra of FVIII bound to PS-vesicles are shown as dotted lines. (b) Ribbon presentation of the of hFVIII-BDD crystal structure superimposed with the pFVIII-BDD homology model. The identical parts in the sequence of both proteins are shown in green. The hFVIII-BDD amino acid residues shown in blue are mutated to the corresponding amino acid residues in the pFVIII-BDD sequence, shown in red. The FVIII domains A1, A2, A3, C1 and C2 are indicated.

Table 2. Secondary structure distribution of hFVIII-FL and pFVIII-BDD in solution and when bound to PS-vesicles. Secondary structure deconvolution of the CD spectra was done with the CONTIN software included in the CDPro package. SMP56 (190–240 nm) was used as a reference protein data set [36].

Sample	α-helices	β-strands	β-turns	random	RMSD
hFVIII-FL	6.3	37.8	22	33.8	0.022
hFVIII-FL+ves	6.4	36.4	22.5	34.7	0.046
pFVIII-BDD	4.7	39.3	22.1	33.6	0.044
pFVIII-BDD+ves	4.6	39.4	22.1	33.8	0.056

PS-vesicles using the same solution conditions as for the CD and Cryo-EM experiments. The average radius of 6 nm, calculated for the human and porcine FVIII-BDD in solution corresponds to the molecular mass of the FVIII-BDD heterodimer ~170 kDa. For the FVIII-FL in solution, the calculated average radius of 9 nm also corresponds to the molecular mass of the predominant hFVIII-FL heterodimer of ~200 kDa. A small fraction of aggregated protein was observed corresponding roughly to the size of three FVIII-FL molecules. The FVIII-BDD forms remained very homogeneous and monodispersed over time (Table 3). The PS-vesicles in solution were equally distributed in two populations with radius of ~50 and ~164 nm, corresponding to the size of the vesicles observed by Cryo-EM (Table 3, Fig. 4a). Upon adding FVIII-BDD to the PS-vesicles, rapid aggregation was observed, which culminated within the first 30 min (Fig. 4c,d). In the absence of PS-vesicles, the FVIII-FL and FVIII-BDD forms did not aggregate in the same solution conditions. Likewise, the PS-vesicles did not show a tendency to aggregate in the absence of FVIII-BDD (Fig. 4a).

Cryo-electron microscopy

Cryo-EM digital micrographs were collected for the control PS-vesicles and the FVIII+vesicle samples at the same conditions as for the CD experiments (Fig. 4). A well-defined membrane bilayer (Fig. 4a) with a thickness of 4.5 nm corresponding to the known thickness of a standard phospholipid bilayer was observed for the 'naked' vesicles (Fig. 5a – histogram). The FVIII-FL+vesicle sample showed well-defined vesicles with tightly packed protein molecules bound at the membrane surface (Fig. 4b). Both human and porcine FVIII-BDD+vesicle samples showed large protein–lipid aggregates with well-defined membrane-bound FVIII-BDD molecules at the extremities (Fig. 4c,d). The height of the membrane-bound protein molecules was calculated at 9.6 nm for all three FVIII forms (Fig. 5b–d: histograms). To better illustrate the organization of the membrane-bound FVIII molecules observed by Cryo-EM, magnified 2D projection maps (100 × 90 pixels at 5.8 Å/pixel) were created and cropped in UCSF-Chimera software [31]. The densities corresponding to one FVIII molecules in these maps were delineated showing the orientation of the FVIII-FL and FVIII-BDD molecules bound to the phospholipids membrane (Fig. 5b–d: third row). No clear difference was observed between the densities for the human and porcine FVIII-BDD heterodimers (Fig. 5, first row). However, there was a consistent difference in the packing between the hFVIII-FL and the FVIIII-BDD forms (Fig. 5, third row). The wider arrangement of the membrane-bound hFVIII-FL molecules, as well as the additional densities observed between the membrane-bound molecules was attributed to the presence of the B-domain's parts attached to the FVIII-HC (Fig. 5b).

Discussion

Comparison of the far UV CD spectra of pFVIII-BDD and hFVIII-BDD confirm that the similarity between the human and porcine FVIII primary sequences

Table 3. Dynamic light scattering of pFVIII-BDD, hFVIII-FL and hFVIII-BDD in solution and bound to PS-vesicles [36]. The size of the particles is shown as mean radius and the polydispersity as a standard deviation (SD). The size distribution by mass represents the distribution of particles according to their mass relative to the total mass of the particles.

Sample	Size (nm)	Mass (%)	Size (nm)	Mass (%)	Size (nm)	Mass (%)	Size, (nm)	Mass (%)
Vesicles			51 ± 9	55 ± 14	164 ± 29	45 ± 18		
hFVIII-FL	9 ± 1	92 ± 3	32 ± 9	8 ± 2				
hFVIII-FL+ves			64 ± 27	40 ± 6	182 ± 23	60 ± 21		
hFVIII-BDD	6 ± 0.2	99 ± 0.1	87 ± 22	1 ± 0.3				
hFVIII-BDD+ves					580 ± 153	48 ± 28	2444 ± 78	52 ± 16
pFVIII-BDD	6 ± 0.3	99 ± 0.2	86 ± 14	1 ± 0.1				
pFVIII-BDD+ves					532 ± 172	39 ± 33	2178 ± 63	61 ± 41

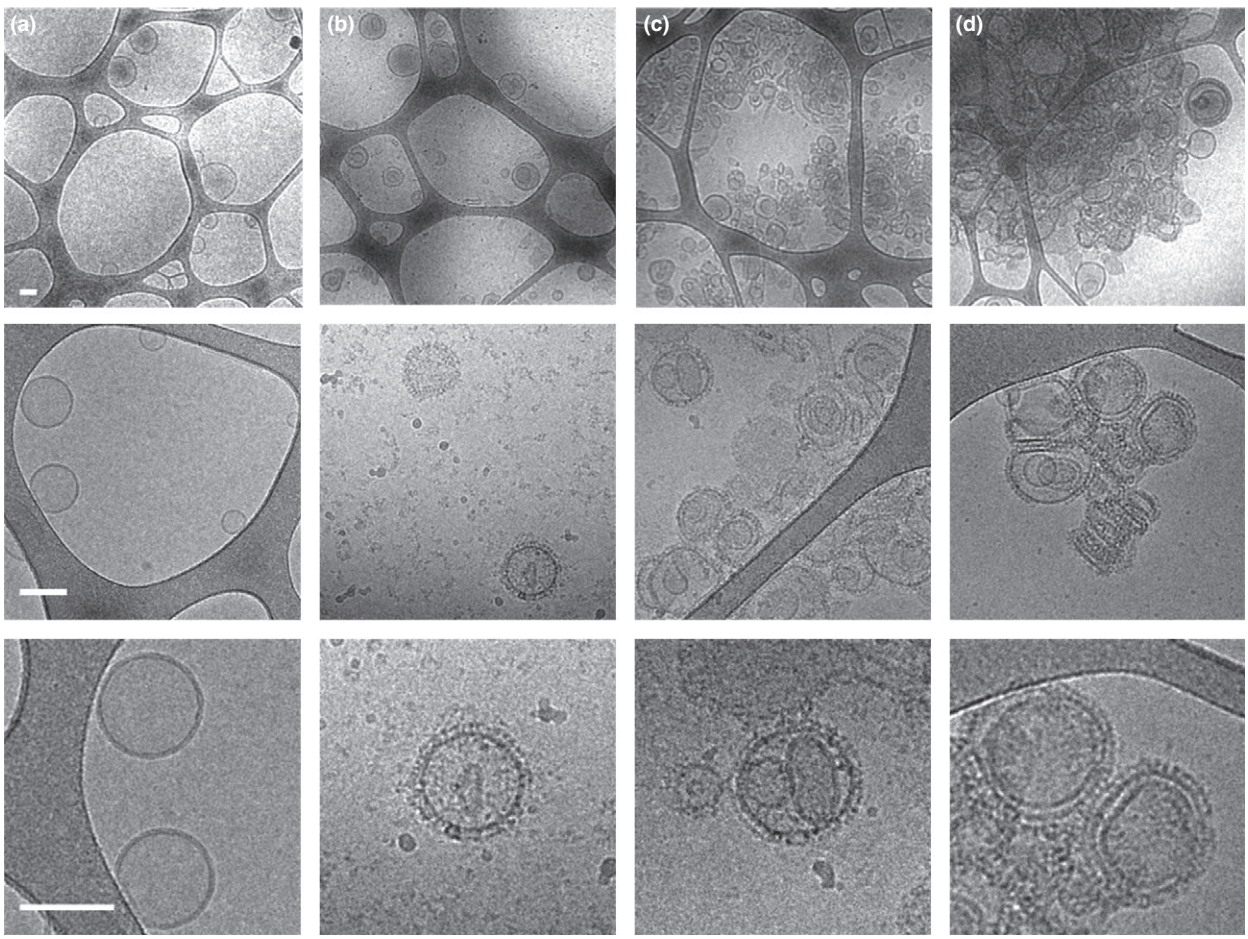

Fig. 4. Cryo-EM digital micrographs of recombinant FVIII forms bound to PS-vesicles recorded at 2.9 Å per pixel. Columns: (a) naked PS-vesicles. (b) hFVIII-FL bound to PS-vesicles. (c) Human FVIII-BDD bound to PS-vesicles. (d) Porcine FVIII-BDD bound to PS-vesicles. The scale bar is 100 nm. The first row shows low magnification view. The third row shows magnified views from the second row.

(86%) extends to a similarity in the secondary and tertiary structures (Fig. 3b). From 224 different amino acids residues, between the human and porcine FVIII-BDD (16% difference in sequence homology), approximately 112 residues (50%) resolved from the hFVIII-BDD crystal structure are located at the protein surface, seven of which at the A2-A3 face supporting the B-domain in the FVIII-FL form (Fig. 3b). The distribution of the amino acid residues, which differs between the human and porcine FVIII-BDD forms explains the similar CD spectra and behaviour upon binding to the PS-vesicles. Binding of both human and porcine FVIII-BDD to PS-vesicles results in fast aggregation of the FVIII-coated vesicles at the concentrations required for the CD and Cryo-EM experiments (~1 mg mL^{-1}). The far UV-CD spectra show that this pronounced aggregation is not due to degradation and denaturation of the proteins, or by any detectable change in the secondary structure. In this case, the observed aggregation appear to be solely due to

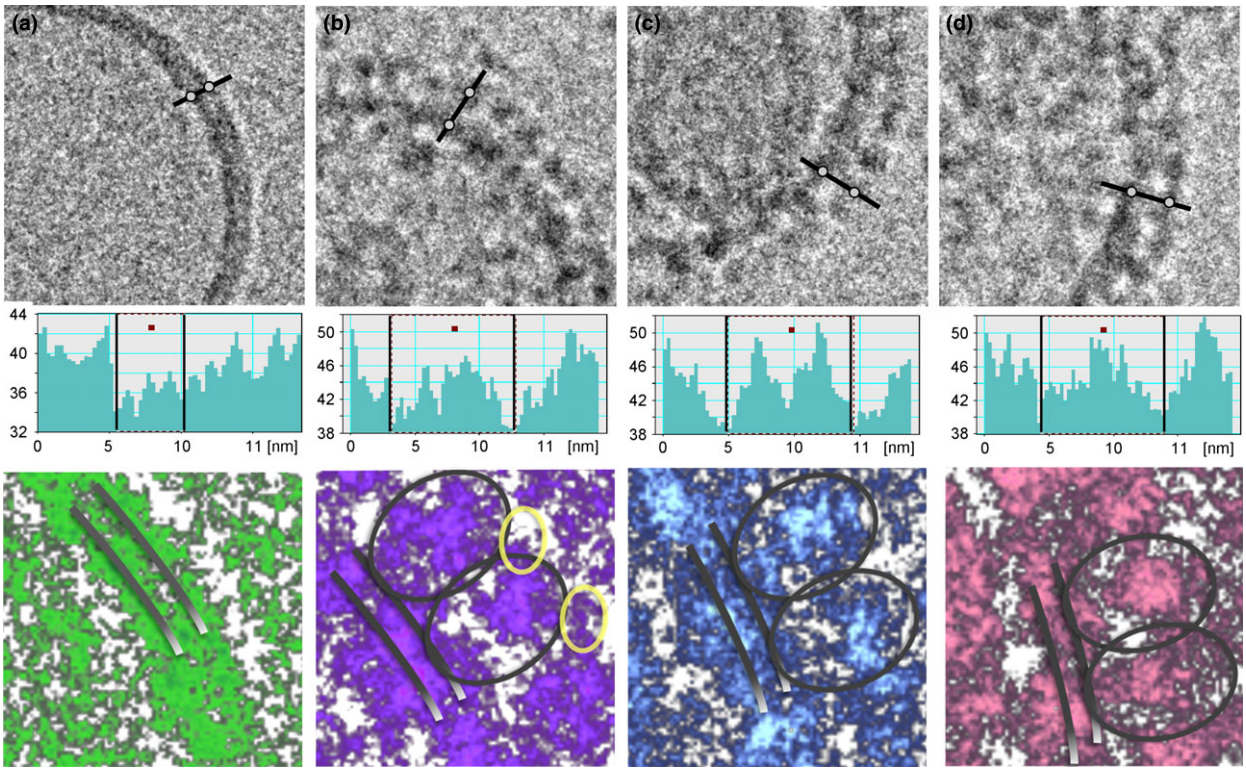

Fig. 5. Magnified Cryo-EM images and corresponding 2D projection maps of recombinant FVIII forms bound to PS-vesicles. Columns: (a) naked PS-vesicles. (b) FVIII-FL bound to PS-vesicles. (c) Human FVIII-BDD bound to PS-vesicles. (d) pFVIII-BDD bound to PS-vesicles. The first row shows magnified views (256 × 256 pixels) from the third row in Fig. 4. The second row shows the histograms (density distribution) of the lipid and protein–lipid mass along the black line drawn on the micrographs in the first row. The distance from minima to minima in (a) is 4.5 nm, in (b), (c) and (d) is 9.6 nm. On the third row are shown the projection maps (projected density distribution) of 100 × 90 pixels areas at 2.9 Å per pixel, selected and rotated from the images in the first row. The centre of density corresponding to the membrane bilayer is indicated with two parallel grey lines. The density corresponding to one membrane-bound FVIII molecule is delineated with a grey oval. The densities corresponding to part of the B-domain present for the membrane-bound FVIII-FL are delineated with yellow ovals (third row, b).

changes in the surface properties of the fully coated FVIII-BDD vesicles, which have a more hydrophobic surface than the uncoated ones. As this effect is not observed for the FVIII-FL, we can conclude that the presence of the whole or part of the B-domain modifies the membrane-bound FVIII face parallel to the membrane surface, preventing the protein induced PS-vesicle aggregation. This is confirmed by the Cryo-EM micrographs that show well-defined FVIII-BDD molecules at the extremity of the aggregates, where the sample is transparent to the electron beam (Fig. 4). The presence of protein aggregates is considered a risk factor for increasing the immunogenicity of therapeutic proteins [32]. A variety of methods are used for testing for protein aggregates are used in the pharmaceutical industry and new methods continue to emerge. FVIII-containing lipid aggregates potentially could form in presence of detergent micelles present as stabilizers in FVIII products or phospholipid microparticles derived from the cells used to produce FVIII during manufacture. Although the immunogenicity of hFVIII-FL and hFVIII-BDD has not been compared in randomized clinical trials, independent prospective studies have not suggested a large difference. However, as new FVIII-BDD products enter clinical testing, differences in formulation could influence immunogenicity. Our study describes novel methods to identify FVIII-phospholipid aggregates that potentially can be applied to the FVIII manufacturing process.

The FVIII-BDD membrane-bound molecules are oriented the same way as the FVIII-FL membrane-bound molecules viewed in a direction parallel to the membrane surface. The wider arrangements of the FVIII molecules and observed extra densities at the extremity of the protein layer suggest that the B-domains which are part of the FVIII-FL heterodimer, disrupt the alignment of the A2-A3 domains face parallel to the membrane surface, rendering the FVIII coated PS-vesicles less hydrophobic and preventing aggregation (Fig. 5).

Cryo-EM is capable of giving direct structural information at subnanometer resolution for fully hydrated samples and close to physiological conditions. Therefore, it is well-suited to study the nature of the FVIII membrane binding and its effect on the PS-vesicle aggregation, and offers a direct visualization of the

membrane-bound FVIII molecules in a functional state. The negative charge of the PS prevents the vesicle aggregation not coated with FVIII. Adding either human or porcine FVIII-BDD masks this charge and promotes aggregation of the FVIII-BDD coated vesicles. The hydrophobicity of the protein-coated vesicle surface is further increased by the close proximity and alignment of the adjacent FVIII molecules. This alignment is disturbed in the case of FVIII-FL by the presence of the B-domain, which protrudes from the FVIII face parallel to the membrane surface at the A2-A3 domains level. Because of the random orientation of the protein molecules, FVIII-BDD does not aggregate in solution, when PS-vesicles are not present. The same height of 9.6 nm measured from the Cryo-EM micrographs for all membrane-bound FVIII molecules (Fig. 5, second row) corresponds to the previously published value for plasma-derived hFVIII organized in membrane-bound 2D crystals [33]. The projected density of the membrane-bound FVIII molecules in the direction parallel to the membrane surface also corresponds to the projected volume in the same direction calculated for the highly homologous membrane-bound factor Va from electron microscopy data [34].

Conclusions

The structural characterization of therapeutic proteins is important for quality control and product release of commercial material. In this study, we have described novel, potentially commercially applicable methods to characterize hFVIII-BDD, hFVIII-FL and pFVIII-BDD both free in solution and in membrane-bound form. Additionally, the membrane binding properties of FVIII are important for its function. The methods of analysis of membrane bound FVIII described in this study could be useful in the future characterization of novel FVIII products designed for improved safety and efficacy.

Acknowledgements

The authors acknowledge the Cryo-EM and solution biophysics facilities at the Sealy Center for Structural Biology UTMB for support, as well as Ms. Christie Shumate for preliminary work on the project. KG performed all biochemical and biophysical experiments and helped with the Cryo-EM samples preparation. JM collected all the Cryo-EM data. DD prepared the pFVIII-BDD homology model. ETP and JFH helped with expression and purification of the FVIII-BDD forms and functional assays. PL critically read the manuscript and helped with the functional data interpretation. SSM designed the work and finalized the manuscript. This work is supported by a National Scientist Development grant from the American Heart Association (10SDG3500034) and UTMB start-up funds to SSM and National Institutes of Health grants U54 HL112309, R01 HL082609 and R01 HL040921 and Hemophilia of Georgia, Inc. to PL.

Disclosures

The authors stated that they had no interests which might be perceived as posing a conflict or bias.

References

1 Soucie JM, Evatt B, Jackson D. Occurrence of hemophilia in the United States. The Hemophilia Surveillance System Project Investigators. *Am J Hematol* 1998; **59**: 288–94.
2 Vehar GA, Keyt B, Eaton D *et al.* Structure of human factor VIII. *Nature* 1984; **312**: 337–42.
3 Toole JJ, Knopf JL, Wozney JM *et al.* Molecular cloning of a cDNA encoding human antihaemophilic factor. *Nature* 1984; **312**: 342–7.
4 Takahashi N, Ortel TL, Putnam FW. Single-chain structure of human ceruloplasmin: the complete amino acid sequence of the whole molecule. *Proc Natl Acad Sci USA* 1984; **81**: 390–4.
5 Kane WH, Davie EW. Blood coagulation factors V and VIII: structural and functional similarities and their relationship to hemorrhagic and thrombotic disorders. *Blood* 1988; **71**: 539–55.
6 Fay PJ. Factor VIII structure and function. *Int J Hematol* 2006; **83**: 103–8.
7 van Dieijen G, Tans G, Rosing J, Hemker HC. The role of phospholipid and factor VIIIa in the activation of bovine factor X. *J Biol Chem* 1981; **256**: 3433–42.
8 Nesheim ME, Pittman DD, Wang JH, Slonosky D, Giles AR, Kaufman RJ. The binding of 35S-labeled recombinant factor VIII to activated and unactivated human platelets. *J Biol Chem* 1988; **263**: 16467–70.
9 Lollar P, Knutson GJ, Fass DN. Stabilization of thrombin-activated porcine factor VIII: C by factor IXa phospholipid. *Blood* 1984; **63**: 1303–8.
10 Pisal DS, Balu-Iyer SV. Phospholipid binding improves plasma survival of factor VIII. *Thromb Haemost* 2010; **104**: 1073–5.
11 Pipe S. Antihemophilic factor (recombinant) plasma/albumin-free method for the management and prevention of bleeding episodes in patients with hemophilia A. *Biologics* 2009; **3**: 117–25.
12 Toole JJ, Pittman DD, Orr EC, Murtha P, Wasley LC, Kaufman RJ. A large region (approximately equal to 95 kDa) of human factor VIII is dispensable for in vitro procoagulant activity. *Proc Natl Acad Sci USA* 1986; **83**: 5939–42.
13 Pittman DD, Alderman EM, Tomkinson KN, Wang JH, Giles AR, Kaufman RJ. Biochemical, immunological, and in vivo functional characterization of B-domain-deleted factor VIII. *Blood* 1993; **81**: 2925–35.
14 Lusher JM. First and second generation recombinant factor VIII concentrates in previously untreated patients: recovery, safety, efficacy, and inhibitor development. *Semin Thromb Hemost* 2002; **28**: 273–6.
15 Gatti L, Mannucci PM. Use of porcine factor VIII in the management of seventeen patients with factor VIII antibodies. *Thromb Haemost* 1984; **51**: 379–84.
16 Hay CR, Lozier JN, Lee CA *et al.* Safety profile of porcine factor VIII and its use as hospital and home-therapy for patients with haemophilia-A and inhibitors: the results of an international survey. *Thromb Haemost* 1996; **75**: 25–9.
17 Kempton CL, Abshire T.C., Deveras R.A. *et al.* Pharmacokinetics and safety of OBI-1, a recombinant B domain-deleted porcine factor VIII, in subjects with haemophilia A. *Heamophilia* 2012; **18**: 798–804.
18 Lollar P, Parker ET. Structural basis for the decreased procoagulant activity of human factor VIII compared to the porcine homolog. *J Biol Chem* 1991; **266**: 12481–6.
19 Doering CB, Healey JF, Parker ET, Barrow RT, Lollar P. High level expression of recombinant porcine coagulation factor VIII. *J Biol Chem* 2002; **277**: 38345–9.
20 Lollar P, Parker CG. Subunit structure of thrombin-activated porcine factor VIII. *Biochemistry* 1989; **28**: 666–74.
21 Ngo JC, Huang M, Roth DA, Furie BC, Furie B. Crystal structure of human factor VIII: implications for the formation of the factor IXa-factor VIIIa complex. *Structure* 2008; **16**: 597–606.
22 Shen BW, Spiegel PC, Chang CH *et al.* The tertiary structure and domain organization

of coagulation factor VIII. *Blood* 2008; **111**: 1240–7.
23 Lind P, Larsson K, Spira J *et al.* Novel forms of B-domain-deleted recombinant factor VIII molecules. Construction and biochemical characterization. *Eur J Biochem* 1995; **15**: 19–27.
24 Pace CN, Vajdos F, Fee L, Grimsley G, Gray T. How to measure and predict the molar absorption coefficient of a protein. *Protein Sci* 1995; **4**: 2411–23.
25 Kirmse R, Bouchet-Marquis C, Page C, Hoenger A. Three-dimensional cryo-electron microscopy on intermediate filaments. *Methods Cell Biol* 2010; **96**: 565–89.
26 Laemmli UK. Cleavage of structural proteins during the assembly of the head of bacteriophage T4. *Nature* 1970; **227**: 680–5.
27 Hemker HC, Giesen P, Al Dieri R *et al.* Calibrated automated thrombin generation measurement in clotting plasma. *Pathophysiol Haemost Thromb* 2003; **33**: 4–15.
28 Emsley P, Cowtan K. Coot: model-building tools for molecular graphics. *Acta Crystallogr D Biol Crystallogr* 2004; **60**: 2126–32.
29 Liu Z, Lin L, Yuan C *et al.* Trp2313-His2315 of factor VIII C2 domain is involved in membrane binding: structure of a complex between the C2 domain and an inhibitor of membrane binding. *J Biol Chem* 2010; **285**: 8824–9.
30 Davis IW, Leaver-Fay A, Chen VB *et al.* MolProbity: all-atom contacts and structure validation for proteins and nucleic acids. *Nucleic Acids Res* 2007; **35**: W375–83.
31 Pettersen EF, Goddard TD, Huang CC *et al.* UCSF Chimera – a visualization system for exploratory research and analysis. *J Comput Chem* 2004; **25**: 1605–12.
32 den Engelsman J, Garidel P, Smulders R *et al.* Strategies for the assessment of protein aggregates in pharmaceutical biotech product development. *Pharm Res* 2011; **28**: 920–33.
33 Stoilova-McPhie S, Villoutreix BO, Mertens K, Kemball-Cook G, Holzenburg A. 3-Dimensional structure of membrane-bound coagulation factor VIII: modeling of the factor VIII heterodimer within a 3-dimensional density map derived by electron crystallography. *Blood* 2002; **99**: 1215–23.
34 Stoilova-McPhie S, Parmenter CD, Segers K, Villoutreix BO, Nicolaes GA. Defining the structure of membrane-bound human blood coagulation factor Va. *J Thromb Haemost* 2008; **6**: 76–82.
35 Shapiro NI, Yano K, Okada H *et al.* A prospective, observational study of soluble FLT-1 and vascular endothelial growth factor in sepsis. *Shock* 2008; **29**: 452–7.
36 Sreerama N, Woody RW. Estimation of protein secondary structure from circular dichroism spectra: comparison of CONTIN, SELCON, and CDSSTR methods with an expanded reference set. *Anal Biochem* 2000; **287**: 252–60.

